The Journal of the Korean Society of
Coastal and Ocean Engineers
Vol. 5, No. 1, pp. 25~38, March 1993

Response of Cable-Buoy Systems to Directional Random Waves
多方向 不規則波浪에 의한 케이블과 浮體시스템의 反應

Sang Soo Jeon** and John. W. Leonard*
全祥秀** · 존 레너드*

Abstract □ Numerical models of directional wave spectra for the analysis of offshore structural cable responses are verified. Alternative spreading models are used to predict wave-induced flows in water and for mooring systems. Hydrodynamic wave forces upon cable are estimated, using a Morison formula encompassing considerations for drag and for inertial forces both parallel and tangential to the slope of the cable. Numerical analysis for directional random waves, including consideration of displacement and velocity, trajectory, phase plane response, and tension are shown for mooring system cable responses at both the tether point for a buoy and at the anchor point. The effects of wave forces for different drag coefficients, various significant wave heights, and selected wave parameters are considered in the analysis. For the specific systems considered in the examples, it is demonstrated that wave period and height, as well as wave spreading function parameters and drag coefficients, have an important effect upon the dynamic responses of the cable-buoy systems.

要 旨 : 해양구조물의 케이블 반응 분석을 위한 다방향 파람 스펙트라의 수치모델이 조사되었다. 여러 형태의 전파모델을 파랑으로 인한 물입자의 흐름과 계류시스템을 예측하기 위해 사용하였다. 케이블에 작용하는 수동역학적 파력은 케이블의 경사에 평행한 방향과 접선방향에서의 항력과 관성력을 고려한 Morison 공식에 의해 평가되었다. 변위와 속도, 궤적, 위상면의 반응, 그리고 장력을 고려한 다방향 불규칙 파랑의 수치해석에 의하여 부체의 tether point와 anchor point에서 계류시스템 케이블의 반응을 나타내었다. 서로 다른 항력계수와 다양한 유의파고, 그리고 선택된 파랑계수들이 이 분석에 고려되었다. 예제에서 고려된 특정 시스템을 통하여 파랑의 전파함수계수와 항력계수 뿐만 아니라 파랑의 주기와 높이가 케이블-부체시스템의 동적반응에 중요한 영향을 미침을 알 수 있었다.

1. INTRODUCTION

The subject of this study is the simulation, for ocean environment, of the nonlinear responses of cables coupled to small bodies such as buoys. Since an increasing number of structures are sited in deep ocean waters in areas subject to hazardous environmental conditions, cable-supported structures have become increasingly important to offshore designers. These structures are commonly subjected to irregular waves which are frequently nonlinear. The kinematic and dynamic analyses of cables in the ocean highly nonlinear and may be attributed to the inherent properties of the cable response, including substantial displacements, lack of compressive stiffness, loading conditions, or other material characteristics. Additional nonlinearities may be introduced for reason of cable position or orientation-dependent loads and boundary conditions. Thus, numerical methods are typically utilized to analyze the deployment of cable systems, including submerged cable arrays with redundant members.

The analysis and design techniques developed for oceanic cable systems were subject to extensive consideration by Chiou (1985), who reviewed the experimentation (Kern *et al.*, 1977; Yashima *et al.*, 1989) on which they were primarily based as well as a number of mathematical models (Webster and Palo,

*오레곤주립대학 土木工學科 (Department of Civil Engineering, Oregon State University, Corvallis, OR 97330; U.S.A.)
**現 現代엔지니어링(株) (Hyundai Engineering Consultant Ltd., Seoul, Korea)

1982; Lo, 1982; Tuah, 1983). It was noted that the use of mathematical models usually results in extensive computer programs that require comprehensive facilities and high computational costs (Leonard and Nath, 1981; Palo, 1985). Thus, the conduct of experimental tests, although invaluable for the provision and validation of data for mathematical models, requires considerable time and expense.

For understanding nonlinear effects in directional spread seas, some progress has been achieved (e.g., Weber and Barrick, 1977). The spreading function for a directional spectrum was evaluated by given data from a tilt and roll buoy (Longuet-Higgins *et al.*, 1963) which were used to determine the first five Fourier coefficients. However, spreading functions obtained by experimental data have a limitation.

Directional spectra can be hindcast using numerical models (e.g., Cardone *et al.*, 1976), and the directional characteristics of hindcast spectra for storms have been verified. Following field measurements taken in the Gulf of Mexico (Forristall *et al.*, 1978), researchers (Niedzwecki and Whatley, 1991) presented the functional forms encompassing the cosine power, exponential and exponential series families of directional spreading functions.

For the current investigation, an algorithm for directional waves (Niedzwecki and Whatley, 1991), is coupled to an algorithm capable of simulating the nonlinear static and dynamic response of a singly-connected cable-body system in three dimensions (Chiou and Leonard, 1991). The configuration of the cable system consists of multiple cable segments and in-line buoys, dynamic responses of which are solved in the time domain. For reason of time evolution, the governing system equations are posed as combined boundary-value and initial-value problems. By introducing a velocity variable, the problem is transformed into the phase domain as a boundary-value problem at a discrete time.

Extensible cable segments are considered and the fluid loading is variable spatially. The hydrodynamic forces from directional waves are calculated by the Morison equation, which considers relative velocity, acceleration, and cable orientation. Subject to the conditions described above, this study focuses upon modelling directional spreading functions to investigate the cable system response in the ocean environment.

By discussion of directional sea models, illustration of similarities and differences between modified-cosine model and wrapped-around Gaussian model is presented. The wave kinematics based on sea models is applied to cable system as a hydrodynamic loading.

2. CABLE AND LOAD MODELS

In general, the statics and dynamics of cable systems are difficult problems to solve from the viewpoint of structural analysis. When they are analyzed for a hostile ocean environment, they are highly nonlinear from the viewpoint of both structural mechanics and hydrodynamics. To deal practically with either an analysis or a design problem, certain simplifying assumptions are necessary. The objective of this section is to set assumptions and to derive the governing equations.

2.1 Basic Assumptions for Cable-Buoy Systems

Cable-buoy systems in this study are subject to the following assumptions:

1) The cable segment is cylindrical in cross-section and is assumed to be a small body in comparison to incident wave lengths. Thus, calculation of the hydrodynamic forces by the Morison equation is valid (Sarpkaya and Issacson, 1981).

2) The cable segment has no flexural or torsional stiffness. Therefore, only uniaxial tension is considered.

3) Only small elastic strains of the cable are considered.

4) Hydrodynamic coefficients for the cable are assumed to be constant.

5) The cable segment may be curved in three dimensions.

6) No cable-bottom interaction is considered. In other words, except at the anchor, the cable segment is assumed to be in the fluid domain at all times.

7) To enable use of linear wave theory, the seafloor is assumed to be flat and impermeable.

8) Intermediate and boundary bodies are assumed

to be small spherical bodies, such that the Morison equation is applicable and hydrodynamic coefficients are the same in all directions.

9) Only translational degrees-of-freedom (i.e, surge, sway, and heave) for the bodies are considered.

10) All cable segments are attached to the centers of gravity of each body.

2.2 Governing Equations for Cable-Buoy Systems

Loads due to gravity, bouyancy and waves for a submerged cable system in the water are considered as environmental loadings. The buoyancy force acts in opposition to the forces due to gravity. Gravity and buoyancy forces are uniformly distributed along the arc length of the cable segment.

Hydrodynamic loads for cable may be grouped in three types: 1) drag forces, 2) inertia forces, and 3) lift forces (note that the latter is not considered for this study). Drag forces are due to skin friction and form drag resulting from vortices or eddies, and from separation of flow. The Morison equation for the estimation of the horizontal wave forces on a fixed vertical pile is written as

$$F=C_I A_I\frac{\partial u}{\partial t}+C_D\ A_D||u|u \tag{1}$$

where

$A_I=\rho\pi D^2/4$
$A_D=\rho\ D/2$
F=hydrodynamic force per unit length of the vertical cylinder
ρ= mass density of fluid
D=pile diameter
C_I=Inertia coefficient
C_D=Drag coefficient

The original Morison equation is empirical. The drag forces may be decomposed into a drag tangent to the cable, and a drag perpendicular to the cable (i.e., in the plane formed by the cable and the relative fluid velocity vector). The drag along the cable is equal to the skin friction of a flat plate having the same surface area as that of the cable.

The drag, perpendicular to the cable consists of both frictional and form drag. For the accelerating fluid, the combination of the drag force and inertia force is given by the semi-empirical Morison equation, in which the in-line drag and inertia coefficients are usually taken as functions of a Reynold's number.

Improvement of the Morison equation in terms of accurately predicting wave forces due to relative water particle velocity and acceleration vectors on small members has been described (Sarpkaya and Issacson, 1981). Using the added mass coefficient, rather than the inertia coefficient, the modified Morison equation including tangential drag term for an oscillating cable in an oscillating flow is described as

$$\begin{aligned}F_i=&\frac{1}{2}\rho\,D\,C_d^n\,|\vec{u}^n-\frac{\overrightarrow{\partial x^n}}{\partial t}|\left(u_i^n-\frac{\partial x_i^n}{\partial t}\right)\\&+\frac{1}{2}\rho\,D\,\pi C_d^t\,|\overrightarrow{u^t}-\frac{\overrightarrow{\partial x^t}}{\partial t}|\left(u_i^t-\frac{\partial x_i^t}{\partial t}\right)\\&+\frac{\pi D^2}{4}\rho(C_a+1)\frac{\partial u_i^n}{\partial t}-\frac{\pi D^2}{4}\rho C_a\frac{\partial^2 x_i^n}{\partial^2 t}\end{aligned} \tag{2}$$

where, C_a is the added mass coefficient and F_i is i^{th} component of hydrodynamic force per unit arclength of cable segment u_i^n, $\partial u_i^n/\partial t$, $\partial x_i^n/\partial t$ and $\partial^2 x_i^n/\partial t^2$ are the components of wave and cable velocity and acceleration normal to its axis, u_i^t and $\partial x_i^t/\partial t$ are the components of wave and cable velocity tangent to its axis.

2.2.1 Cable Segments

The equilibrium equation for dynamic forces on an infinitesimal length dS at an arbitrary material point along the cable segment is defined as (Ablow and Schechter, 1983)

$$\frac{\partial}{\partial S}\vec{T}+\frac{1}{(1+\varepsilon)}\vec{W}_b+\vec{F}+\frac{1}{(1+\varepsilon)}\vec{I}=0 \tag{3}$$

where

S =the arc length along the stretched cable,
$\vec{T}$ =the tension,
$\vec{W}_b$=the buoyant weight per unit length of unstretched cable,
$\vec{F}$ =the hydrodynamic loads per unit stretched length,
$\vec{I}$ =the d'Alembert force, and
ε =the strain.

2.2.2 Boundary Body

Assuming a small spherical body for the boundary body, the Morison equation is used to calculate hydrodynamic forces due to waves. The equilibrium equation for the boundary body may be written as (Chiou, 1989)

$$-(M+\rho C_A V)\frac{\partial^2 X_i}{\partial t^2}+(C_A+1)\rho V\frac{\partial u_i}{\partial t}+\rho_{qqi}+P_i(t)+P_{oi}+W\delta_{1i}-K(X_i-X_i^s)\pm T_i=0 \quad i=1,\ 2,\ 3 \tag{4}$$

where

M = total mass of the intermediate body,
W = wet weight of the intermediate body,
V = volume of the intermediate body,
C_A = added mass coefficient (i.e., the same in all directions),
q_i = $u_i+v_i+X_i$; i^{th} component of relative velocity,
q = $(q_k\ q_k)^{1/2}$, k=1, 2, 3,
β = 0.5 ρ A_o C_D,
A_o = drag area of the intermediate body (i.e., the same in all directions),
C_D = drag coefficient of the intermediate body (i. e., the same in all directions),
K = stiffness constant of the spring that may be attached to the intermediate body,
X_i^s = coordinate where the spring is unstretched,
$P_i(t)$ = time-dependent concentrated load, and
P_{oi} = constant concentrated load.

There is only one cable attached to the boundary body. The selection of the sign of T is dependent upon the location of the boundary body. The positive sign is chosen if the body is located at the starting end of the cable segments relative to the assigned direction of the cable scope coordinate; the negative sign is used if the body is located at the terminal end of the cable segment. The nonlinear interactions between the body and the cable need to be addressed.

2.3 Proposed Directional Sea Models

2.3.1 Directional Spectra

It is common to express the directional spectrum with the unidirecitonal spectrum in the form of a frequency-dependent term multiplied by a spreading term,e.g.

$$S(f,\theta)=S(f)\ H(f,\theta)\ d\theta \tag{5}$$

where

$$\int_{-\pi}^{\pi} H(f,\theta)\ d\theta=1 \tag{6}$$

This indicates that no energy is added by the spreading function, $H(f,\theta)$ rather that it is a mechanism to distribute the energy of the unidirectional spectrum over the specified range of angles $[-\pi, +\pi]$. The spreading funciton, $H(f,\theta)$, in conjunction with an unidirectional spectrum redistributes wave energy by a lower peak height.

The spreading parameter s and the mean peak direction θ_o which depends on the frequency are obtained from published data (Niedzwecki and Whatley, 1991)

$$s(f)=0.0547\ f^{-2.23} \tag{7}$$

$$\theta_o(f)=143.1\ f^{-0.305} \tag{8}$$

2.3.2 Forristall (modified cosine) Model

The modified-cosine model, $H_1(f,\theta)$, of the spreading functions with parameters obtained by field measurements for modified Longuet-Higgins type of cosine-power spreading function

$$H_1(f,\theta)=\frac{\Gamma[s(f)+1]}{2\sqrt{\pi}\Gamma\left[S(f)+\frac{1}{2}\right]}\cos^{2s(f)}[\theta-\theta_o(f)] \tag{9}$$

and the gamma function is defined by the integral

$$\Gamma(z)=\int_o^\infty t^{z-1}e^{-t}\ dt. \tag{10}$$

2.3.3 Wrapped-around Gaussian Model

The wrapped-around Gaussian model, $H_2(f,\theta)$, of the spreading function has an exponential form based on a normal distribution. It is written as

$$H_2(f,\theta)=\frac{1}{2\,\mathrm{erf}\left[\frac{\pi}{2\sigma(f)}\right]-1}\sum_{-k}^{k}\frac{1}{\alpha 2\pi\ \sigma(f)}e^{-1/2\left(\frac{\theta-\theta_o(f)-2\pi k}{\sigma(f)}\right)} \tag{11}$$

where σ is the spreading standard deviation and k represents the number of terms in the series ex-

pansion. Moreover,

$$\mathrm{erf}(x)=\frac{1}{\alpha 2\pi}\int_{-\infty}^{x} e^{-(t^2/2)}\,dt \tag{12}$$

which is the standard error function. The error function is a special case of the incomplete gamma funciton and may be obtained with moderate efficiency. The definition of the error function is

$$e_1(x)=\frac{2}{\alpha\pi}\int_{o}^{x} e^{-t^2}\,dt \tag{13}$$

and the standard error function can be expressed in terms of the error function:

$$\mathrm{erf}(x)=\frac{1}{\sqrt{2\pi}}\int_{-\infty}^{x} e^{-(t^2/2)}\,dt$$
$$=\frac{1}{2}\left(1+e_1\left[\frac{x}{\sqrt{2}}\right]\right) \tag{14}$$

For the wrapped-around Gaussian model, there are only two parameters which must be specified. The parameter, k, represents the number of terms in the series used to model and the wave spread, and the parameter, σ, is similar to the spreading parameter s in the modified-cosine model. The term σ(f) is defined by (Niedzwecki and Whatley, 1991)

$$\sigma(f)=4.95f-0.042. \tag{15}$$

Niedzwecki and Whatley (1991) suggest five terms, k=5, as being generally adequate for computation.

2.3.4 Circular-normal Model

The circular-normal model $H_3(f,\theta)$ of the spreading function is of the form

$$H_3(f,\theta)=N(f)\left[\frac{a(f)}{2\pi}\right]^{1/2} e^{-(a/2)[\Theta-\Theta_o(f)]2} \tag{16}$$

where

$$a(f)=0.037\ f^{-2.117} \tag{17}$$

and the normalizing factor is

$$N(f)=\frac{\left[\frac{2\pi}{a(f)}\right]^{1/2}}{\int_{\pi}^{\pi} e^{-(1/2)[\Theta\ \Theta_o(f)]2}\,d\theta} \tag{18}$$

The form of the normalizing factor can be expressed in terms of an error funciton as

$$\int_{\pi}^{\pi} e^{-(1/2)[\Theta-\Theta_o(f)]2}\,d\theta=\frac{\alpha\pi}{\sqrt{2}}$$
$$\left(e^{1}\left[\frac{(\pi-\theta_o(f))}{\sqrt{2}}\right]+e_1\left[\frac{(\pi+\theta_o(f))}{\sqrt{2}}\right]\right) \tag{19}$$

Therefore,

$$N(f)=\frac{2}{\sqrt{a(f)}\left(e_1\left[\frac{(\pi-\theta_o(f))}{\sqrt{2}}\right]+e_1\left[\frac{(\pi+\theta_o(f))}{\sqrt{2}}\right]\right)} \tag{20}$$

Niedzwecki and Whatley (1991) state that the normalization factor given by eq. (18) is very close to unity for all values of a(f). However, by computation with eq. (20), one sees that the normalization factor is much greater than unity. Since the spectral density is amplified by the normalization factor, the circular-normal model was not considered further in the present work.

2.4 Estimation of Directional Spectra

The angular distribution is very narrow for the frequency components near the spectral peak frequency, whereas it widens rapidly toward higher and lower frequencies. In addition, the mean direction of the dominant spectral component is almost the same as that of the wind. Therefore, in a generating area, it may be said that frequency components near the dominant peak of the frequency spectrum, that is, the frequency components containing the greatest amounts of energy, propagate in nearly the same direction as the wind direction and that their angular spread is very narrow. However, angular spreading increases toward higher and lower frequencies as the spectral energy is decreased. Fig. 1 shows the results of including both the s(f) and $\theta_o(f)$. The consine squared spread for short period waves, and the cosine-eighth spread for swells are illustrated in Fig. 3 through 2.10.

A comparison of the contours for a directional sea spectrum using the wrapped-around Gaussian model, where σ=.6 and variable σ(f), is presented in Fig. 7. The parameter, σ, which depends on the frequency generates more rounded and peaked spectrum. The value σ=.6 apears to be a good estimate.

The various parameters of the spreading functions

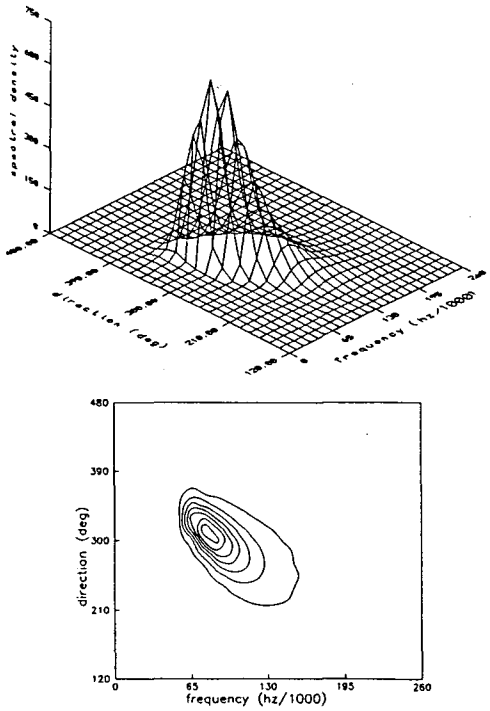

Fig. 1. Directional wave spectrum for the modified cosine spreading function and Bretschneider spectrum for the variable $\theta_0(f)$.

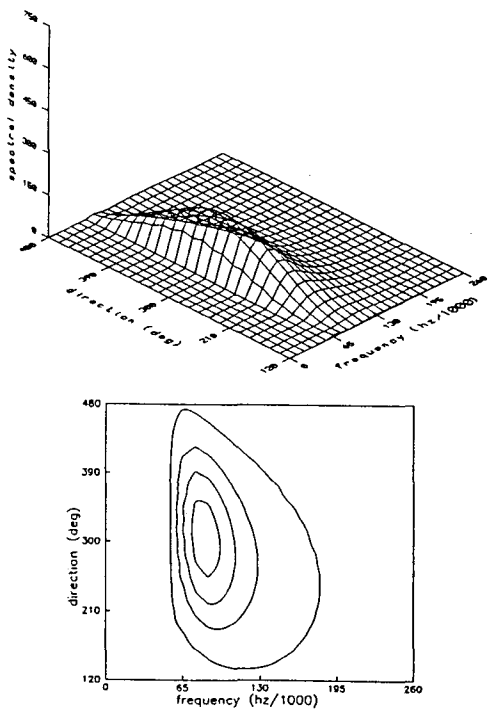

Fig. 3. Directional wave spectrum based on cosine-squared spreading function and Bretschneider spectrum for the variable $\theta_0(f)$.

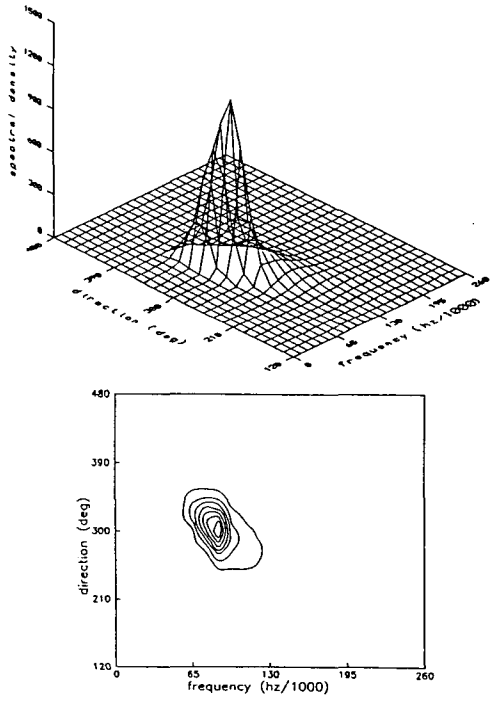

Fig. 2. Directional wave spectrum based on the wrapped-around Gaussian spreading function and the Jonswap spectrum for the variable $\theta_0(f)$.

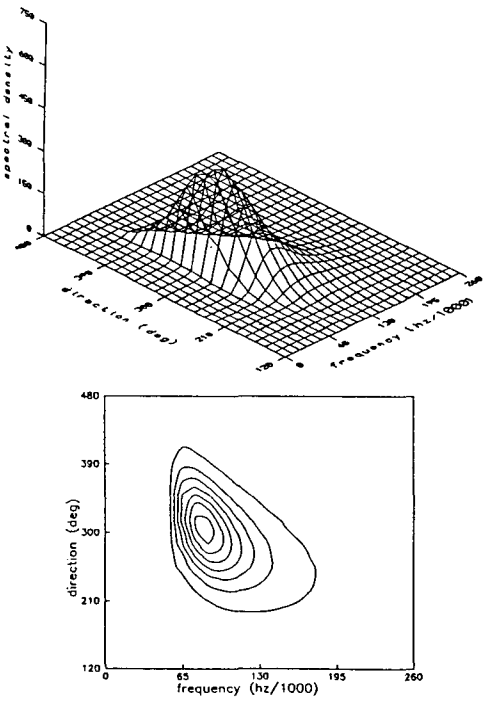

Fig. 4. Directional wave spectrum based on cosine-eighth spreading function and Bretschneider spectrum for the variable $\theta_0(f)$.

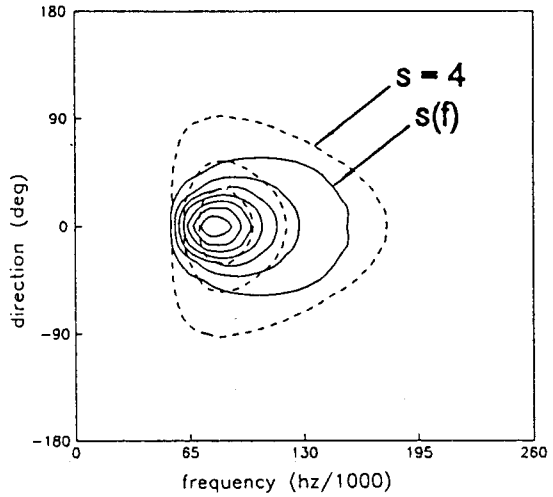

Fig. 5. Comparison of contours for modified cosine spreading and cosine-squared spreading based on the Bretschneider spectrum for $\theta_0(f)=0$.

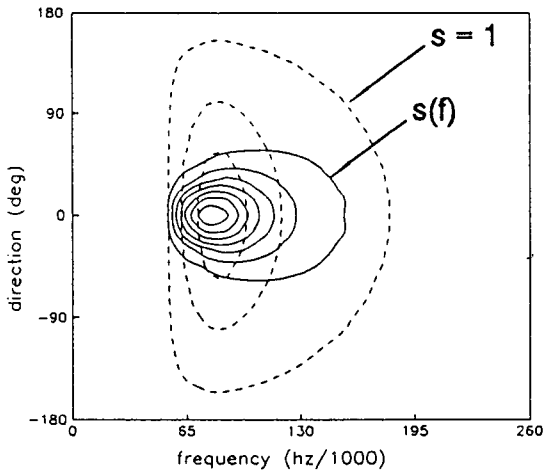

Fig. 6. Comparison of contours for modified cosine spreading and cosine-eighth spreading based on the Bretschneider spectrum for $\theta_0(f)=0$.

have significant effects on the energy distribution between frequency and angular spreading. Since the spreading functions for directions, the responses of the presented directional sea models are expected to be close to one another.

2.5 Irregular Wave Kinematics and Spectral Density by FFT

2.5.1 Monte Carlo Simulation of Irregular Waves

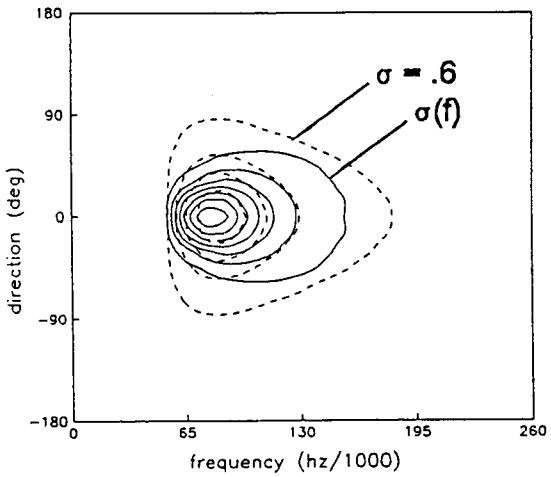

Fig. 7. Comparison of contours for five-term wrapped-around Gaussian spreading based on the Bretschneider spectrum for $\sigma=0.6$.

Over both space and time, the various linear properties of the irregular wave train are assumed to follow the law of multivariate normal probability. Within this framework, conditional probability laws are themselves multivariate normal, thus an elaborate theory can be constructed.

The wave properties that were not measured are stochastic processes which to some degree may be correlated with measured data. Dependent upon the extent and the quantity of the actual data, nonmeasured wave properties may be either constrained to strong agreement with the measurements or only weakly related.

2.5.2 Wave Kinematics

An accurate assessment of water particle kinematics below the surface of the waves is necessary to determine hydrodynamic forces on the cable systems. The simulation for sea surface having a drectional spectral density, $S(f,\theta)$ is given as

$$\eta(x,y,t)=\sum_{m=1}^{M}\sum_{n=1}^{N}A_{mn}\cos(k_m x\cos\theta_n+y\sin\theta_n)-2\pi ft+\phi_{mn}) \quad (21)$$

where

$$A_{mn}=\sqrt{2S(f_m,\theta_n)\,\Delta\theta_n\,\Delta f_m}$$

(x,y,z) rectangular coordinate system. The origin

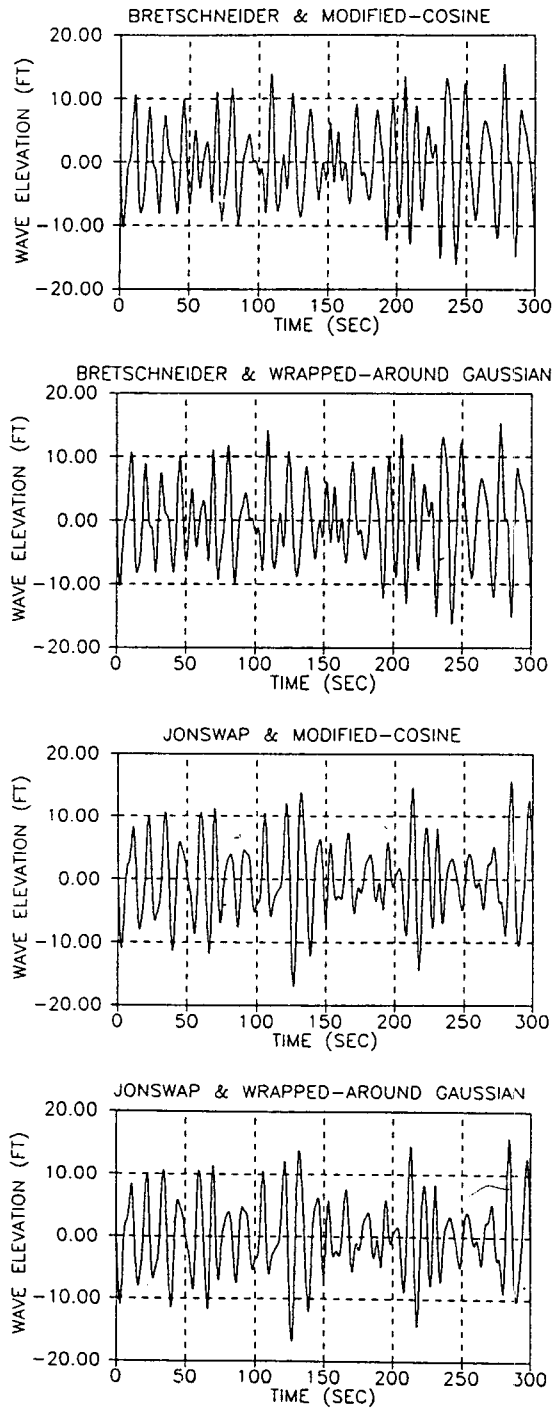

Fig. 8. Random wave profiles.

is at the still water level and x ($-x_3$) is positive northward, y ($-x_2$) positive westward and z($-x_1$) positive upward.

f_m wave frequency in cycles per second
k_m wavenumber associated with frequency
θ_n direction the wavelet is travelling as measured clockwise from the x axis
ϕ_{mn} a random phase for the (m, n) wavelet assumed to be uniformly distributed over the angles $(0, 2\pi)$ and independent from wavelet to wavelet
A_{mn} amplitude of the (m, n) wavelet
$S(f, \theta)$ directional spectral density at frequency and direction
Δf_m frequency interval about frequency f_m
$\Delta\theta_n$ angle interval about travel direction θ_n

Fig. 8 displays for different combination of unidirectional spectral models and spreading functions the Monte Carlo simulations of surface elevation due to irregular waves. The wave kinematics can be obtained from linear wave theory so that

$$u(x,y,z,t)=\sum_{m=1}^{M}\sum_{n=1}^{N}\eta(x,y,t)\,(2\pi fm)\frac{\cosh k_m(d+z)}{\sinh k_m d}\cos\theta_n \tag{22}$$

$$a(x,y,z,t)=\sum_{m=1}^{M}\sum_{n=1}^{N}\eta(x,y,t)\,(2\pi fm)^2\frac{\cosh k_m(d+z)}{\sinh k_m d}\sin\theta_n \tag{23}$$

where u(x,y,z,t) is the water particle velocity at space location (x,y,z) and at time t, and a(x,y,z,t) the water particle acceleration. The number of included frequencies was selected M=50, and the number of angles as, N=37 for use in calculations in this work.

The fast Fourier transform is achieved by discretizing time and frequency,

$$t=n\Delta t,\ n=0,\ 1,\ 2,\cdots,\ N\text{-}1,$$
$$f_m=m\Delta f,\ m=0,\ 1,\ 2,\cdots,\ N/2 \tag{24}$$

where the time and frequency increments are taken to satisfy

$$(\Delta t)(\Delta f)=1/N \tag{25}$$

The time series formula simulated by the Monte Carlo method, as represented in the frequency domain by FFT, becomes

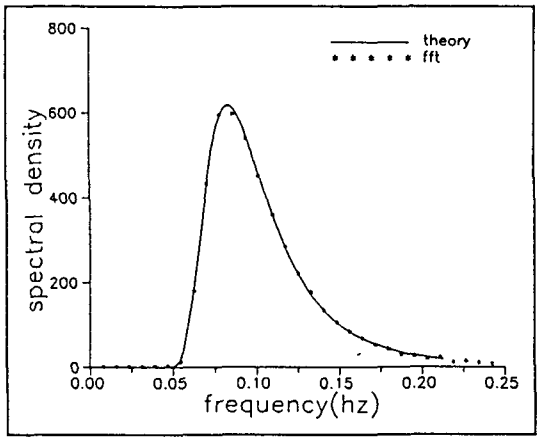

Fig. 9. Comparison of Bretschneider spectrum based on the modified cosine spreading function from theory and as obtained By FFT.

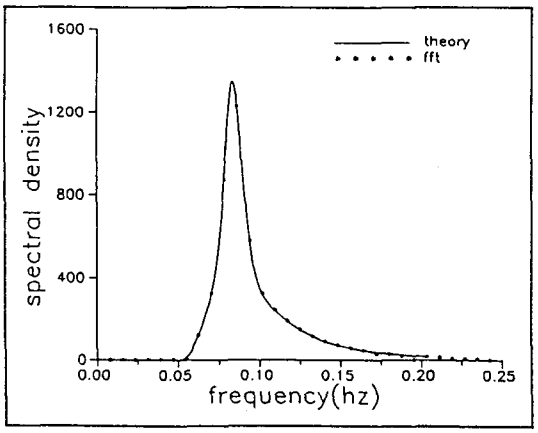

Fig. 10. Comparison of Jonswap Spectrum based on the wrapped-around Gaussian spreading function from theory and as obtained By FFT.

$$B(m\Delta f,x,y,z)=\sum_{M=0}^{N-1} b(n\Delta t;x,y,z)\ \exp(i2\pi mn/N) \quad (26)$$

The unidirectional spectrum can be obtained by squeezing the spectral density at each frequency of the directional spectrum. Comparisons between the theoretical spectrum with the spectrum obtained by FFT from generated waves in the frequency domain are shown in Figs. 2.13 and 2.14 for two combination of spreading functions and spectrum models. Good agreement is seen in both cases.

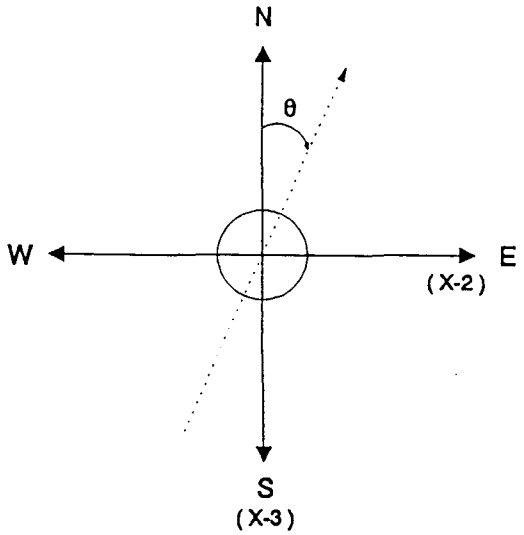

Fig. 11. Single-point mooring and rectangular coordinate system.

3. CABLE RESPONSES TO VARIOUS MODELS

3.1 Description of the Problem

The cable responses for a single-point mooring system of a buoy are used to demonstrate the deterministic dynamic analysis procedure for a hydrodynamically loaded cable-body system. The examples have reference to a single, linearly elastic cable attached to a small body under the water, with the cable initially stretched from the bottom of the ocean, as shown in Fig. 11. The buoy was considered to be statically displaced to a specified equilibrium position and then to respond to directional random waves. The dynamic responses of the mooring system were calculated. Horizintal cable motion is the single most significant behavior parameter for the case of a cable exposed to a random beam sea environment. Small high frequency fluctuations in vertical cable amplitudes are noted, but in most cases may be disregarded since they are not germane to the problem under consideration. The high frequency vertical motion is due to the elastic waves propagating along the cable. The lower frequency lateral motions are forced by the waves. The general case developed for this study is described as follows:

1) Cable Data:
   Unstretched length=594 ft,
   Weight in Water=0.0 lb/ft,
   Diameter=0.057 ft,
   Tangential drag coefficient=0.02,
   Normal drag coefficient=1.2,
   Added mass coefficient=1.0,
2) Buoy Data:
   Diameter=2.5 ft,
   Weight in air=438.37 lbs,
   Weight in fluid=−4214.96 lbs,
   Drag coefficient=.5, and
   Added mass coefficient=.5,
3) Wave/fluid data:
   Fluid depth=620 ft,
   Fluid density=2.0 slugs/ft3,
   Spectrum=Bretschneider or Jonswap,
   Spreading model=Modified-cosine or Wrapped-around,
   Angle step of spreading functions=10°,
   Significant wave height=24 ft,
   Dominant wave period=12 secs,
4) Numerical integration data:
   Initial configuration by static analysis
   Cable segments=41,
   Non-dimensional error tolerance=0.05,
   Time length=30 or 300 secs,
   Time step=0.25 or 0.30 sec

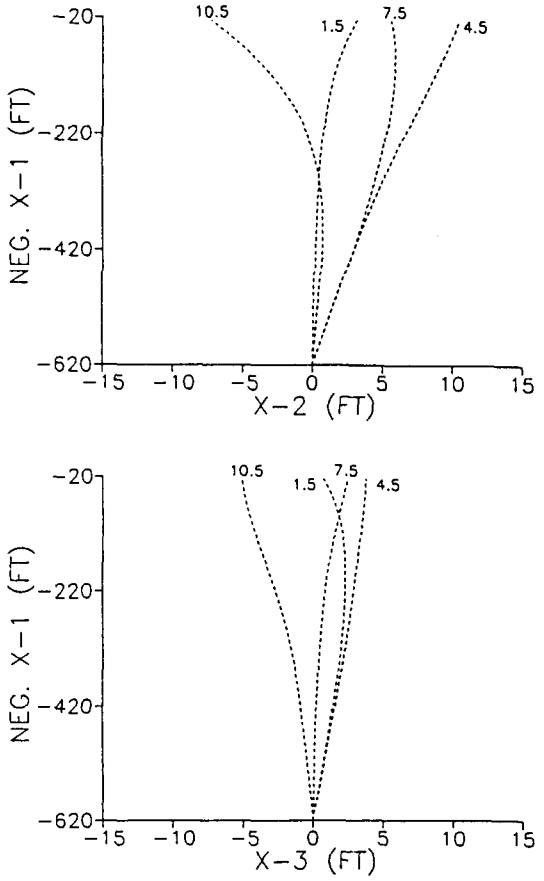

Fig. 12. Lateral profiles of single-point mooring system (1.5 to 10.5 seconds).

The validation of the proposed sea models for the three-dimensional and nonlinear dynamic analyses of a singly-connected cable-body system is demonstrated by consideration of a series of example problems. Steady environmental loadings from winds are calculated by the methods previously considered in section 2 and wave forces are generated using either Bretschneider or Jonswap wave spectrum equations, combined with either modified-cosine or wrapped-around Gaussian spreading functions. Numerical results are obtained for this application through the medium of a computer program developed for this study and based upon the models in section 2. Fig. 12 plots the two vertical system profiles during two cycles of wave forces, based upon the combined Bretschneider spectrum model and modified-cosine model. Numbered labels on each profiles denote time in secs. Vertical and horizontal movements are indicated during the cycles at the end points of all 41 cable segments. Note how the profile changes shape.

3.2 Example Results for Bretschneider Spectrum/ Modified-Cosine Model

Time histories for the vertical and horizontal cable displacements and velocities are shown, respectively, in Fig. 13 and 14. Vertical reflected vibration because of elastic wave travelling along the cable. Note the small amplitudes of motions. The response frequency of cable for wave frequency was nearly identical. Compared to the magnitudes of the vertical displacements, the magnitudes of horizontal displacements are large. In Fig. 14, the horizontal velocity of the magnitudes of horizontal displacements are large. In Fig. 14, the horizontal velocity of the

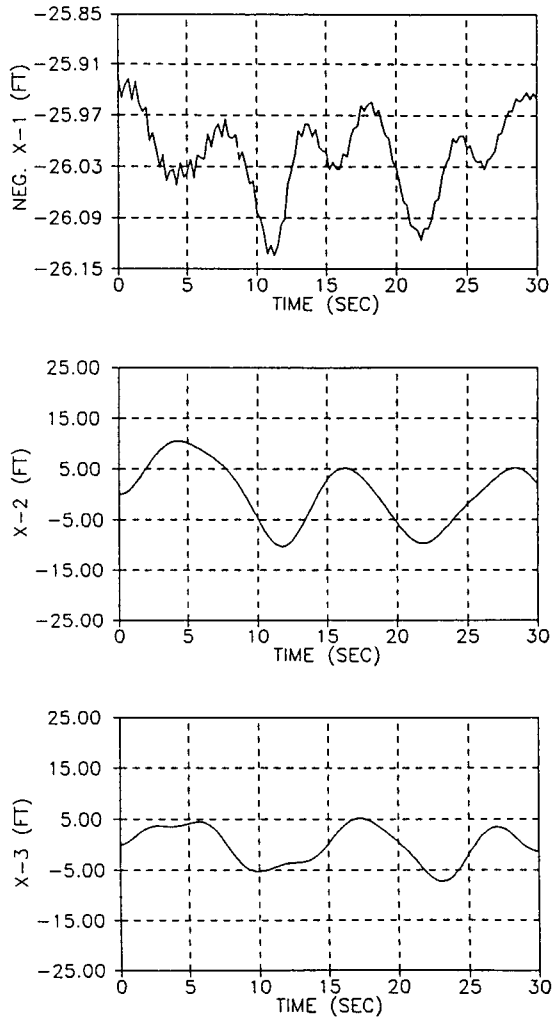

Fig. 13. Time histories for cable motions at tether point for example.

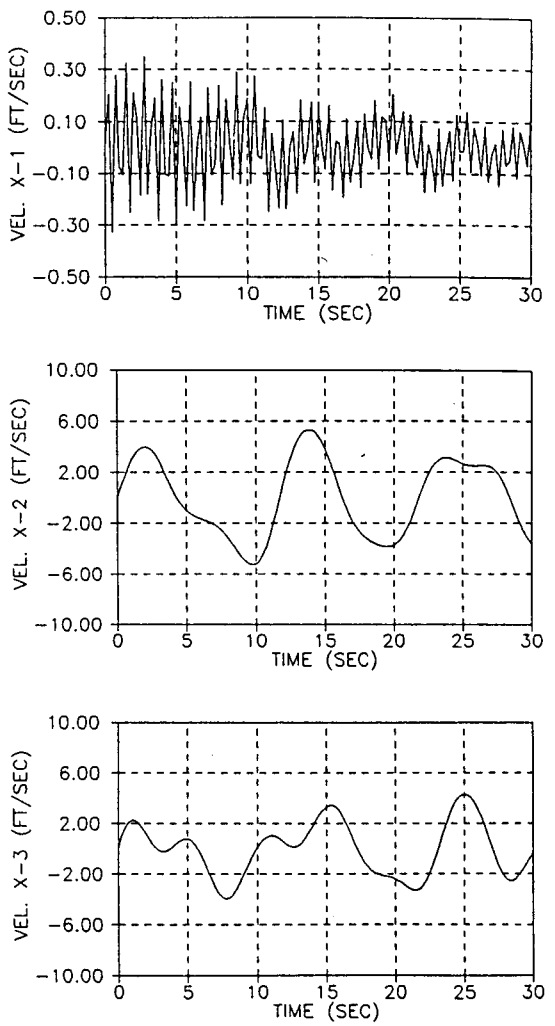

Fig. 14. Time historices for cable velocities at tether point for example.

water particles caused the mooring cables to curve such that the buoy was forced to move downward. At the buoy, buoyancy tended to stretch the mooring cable, imparting an upward motion to the buoy when the horizontal velocity of the water particles changed directions. Thus, there exists a dominant period in the vertical motion at the wave period, as can be shown in Fig. 13.

Fig. 15 shows the trajectories of the cable at the tether point in two planes, indicating a response frequency similar to that for waves; that is, a directionality corresponding to both wave direction and vertical vibration. Fig. 16 shows the vertical and horizontal responses of the cable in the phase planes (i.e., directionality). What is not indicated in these figure views is that the system approached steady-state following the application of a certain number cycles of wave forces. Tension responses at the anchor and at the tether for horizontal components are presented in Fig. 17.

Since the initial horizontal vibration occurred principally near the surface of the water, a phase delay can be seen in the tension response at the anchor; thus, tension responses at the anchor and at the tether point reflect different phases. The vertical tension range was from 2700 to 4900 lbs; the

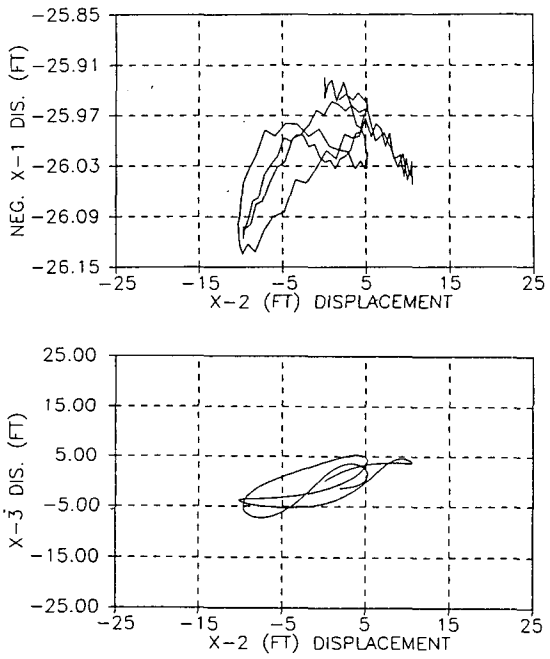

Fig. 15. Cable trajectories at the tether point for example.

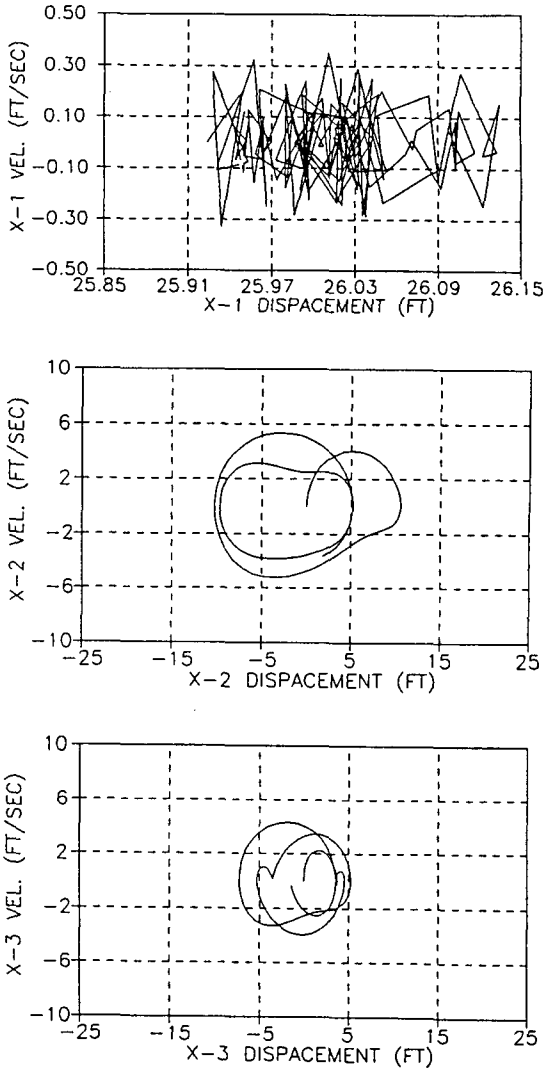

Fig. 16. Phase plane responses of the cable at the tether point for example.

range of the magnitude of the horizontal tension was 200 lbs; and the magnitude of horizontal displacement and vertical tension was much larger, respectively, than the magnitude of vertical displacement and horizontal tension.

4. EVALUATION OF RESULTS

The purpose of this investigation was to consider the effect of mooring line dynamics for the response analysis of submerged cable systems affected by random directional wave actions. The results of the investigation indicated that to accurately predict cable system performance and to realistically evaluate cable responses for the type of system considered, the effect of cable dynamics must be considered for a comprehensive dynamic system analysis. For the model considered, the inherently dynamic nature of the problem, including large displacements and position-dependent nonlinear hydrodynamic forces, was accommodated. Thus, by means of this approach to determination of the effects of cable dynamics, a basis has been provided for the feasible solution of cable dynamics problems as well as the improvement of cable system design methodologies.

By means of the example problems considered in section 3, the responses presented demonstrated predictions for the dynamic behaviors of cable segments that show directionality. However, during testing of the computer simulation program based upon analysis of the proposed model, certain problems were encountered. The selection of a time-step is the most sensitive factor in this type of numerical analysis.

As reviewed in section 1, the consideration of di-

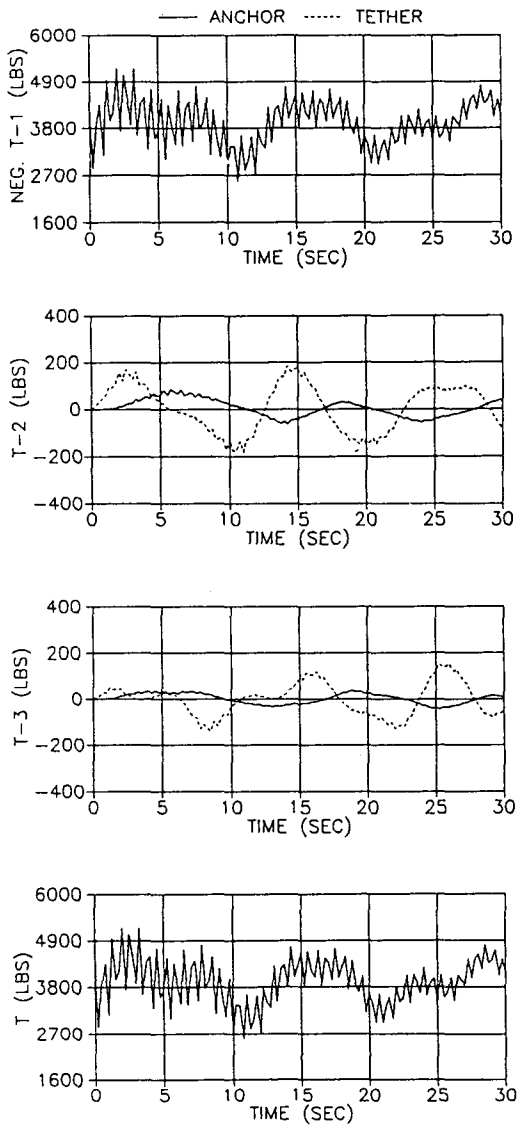

Fig. 17. Tension time histories at the tether point and at the anchor point for example.

rectional seaways for the design of offshore has been indicated. There has been little verification of the directional charateristics of the hindcast spectra using numerical models. In any event, the directional random waves produced by spreading functions, which are the frequency dependence of various model parameters and coupling between frequencies and angular spreads, have a significant effect on the cable response. Therefore, the directional random waves should be considered in the design of mooring system.

ACKNOWLEDGEMENTS

This study was supported in part by the Naval Civil Engineering Laboratory contract no. N 47408-90-C1149.

REFERENCES

Ablow, C.M. and Schechter, S., 1983. Numerical simulation of undersea cable dynamics, *Ocean Engineering*, **10**: 443-457.

Bathe, K.J., 1984. Finite element procedures in engineering analysis, Prentice-Hall, Englewood Cliffs, NJ.

Borgman, L.E., 1969. Ocean waves simulation for engineering design, *Journal of the Waterways and Harvors Division*, **95**: 557-583.

Cardone, V.J., Pierson, W.J. and Ward, E.G., 1976. Hindcasting the directional spectra of hurricane-generated waves, *Journal of Petroleum Technology*, **25**: 385-394.

Chiou, R., 1989. Nonlinear static analysis of long submerged cable segments by spatial integration, M.S. thesis, Oregon State University.

Chiou, R., 1989. Nonlinear hydrodynamic response of curved singly-connected cables, Ph.D. Dissertation, Oregon State University.

Chiou, R. and Leonard, J.W., 1991. Nonlinear hydrodynamic response of curved singly-connected cables, *Proceedings, Computer modelling in OceanEngineering*, at Barceloca, Spain, Oct. 417-424.

Forristall, G.Z., 1978. On the statistical distribution of wave heights in a storm, *Journal of Geophysical Research*, **83**: 888-909.

Forristall, G.Z., Ward, E.G., Cardone, V.J. and Borgman, L.E., 1978. The directional spectra kinematics of surface gravity waves in tropical storm Delia, *Journal of Physical Oceanography*, **8**: 888-909.

Kern, E.C., Jr., Milgram, J.H. and Lincoln, W.B., 1977. Experimental determination of the dynamics of a mooring system, *Journal of Hydronautics*, **11**: 113-120.

Leonard, J.W., 1988. Behavior and analysis of tension structures, McGraw-Hill, New york.

Leonard, J.W. and Nath, J.H., 1981. Comparison of finite element and lumped parameter methods for ocean cables, *Engineering Structures*, **3**: 153-167.

Lo, A., 1982. Nonlinear dynamic analysis of cable and membrane structures, Ph.D. Dissertation, Oregon State University.

Longuet-Higgins, M.S., Cartwright, D.E. and Smith; N.D., 1963. Observations of the directional spectrumo of sea waves using the motion of a floating buoy, in *Ocean Wave Spectra* (pp. 111-136), Prentice-Hall, Englewood Cliffs, New Jersey.

Niedzwecki, J.M. and Whatley, C.P., 1991. A comparative

study of some directional sea models, *Ocean Engineering* **18**: 111-128.

Palo, P.A., 1985. Development of a general-purpose mooring analysis capability for the U.S. Navy, paper presented at the meeting of the San Diego Section, Society of Naval Architects and Marine Engineers, February.

Rayleigh, J.W.S., 1945. Theory of Sound, 2nd ed., Vol. I, Dover Publications, New York.

Sarpkaya, T. and Issacson, M., 1981. Mechanics of Wave Forces on Offshore Structures, Van Nostrand Reinhold Company, New York.

Tuah, H., 1983. Cable dynamics in an ocean environment, Ph.D. Dissertation, Oregon State University.

Weber, B.L. and Barrick, D.E., 1977. On the nonlinear theory for gravity waves on the ocean's surface, Part I: Derivations, *Journal of Physical Oceanography*, 7: 3-10.

Webster, R.L. and Palo, P.A., 1982. SEADYN User's Manual, *NCEL Technical Note N-1630*, Port Hueneme, CA.

Yashima, N., Matsunaga, E. and Nakamura, M., 1989. A large-scale model test of turret mooring system for floating production storage offloading (FPSO), *OTC 5980*, Offshore Technology Conference, Houston, TX, 223-232.